*A NEW GENERIC SENSOR ORIENTATION MODEL APPLIED TO ALOS IMAGERY**

C.S. Fraser, F. Rottensteiner, T. Weser and J. Willneff
Cooperative Research Centre for Spatial Information, Department of Geomatics
University of Melbourne, VIC 3010, Australia
{c.fraser, franzr, tweser, jochenw}@unimelb.edu.au

Abstract
This paper will present the results of experimental applications of a new, generic sensor orientation model for pushbroom imaging sensors to ALOS PRISM imagery. Within the model, which has been incorporated into the BARISTA software system for metric information extraction from satellite imagery, the sensor orbit and attitudes are modelled by splines. In order to determine the parameters of the splines, direct vendor-provided observations for the satellite orbits and attitudes, available in the metadata files, are employed. These direct observations are usually contaminated by systematic errors and so a rigorous model is used to compensate perturbations in the orbit and attitude data. The new sensor model has been designed to be applicable to a large variety of sensors, with satellite-specific definitions being mapped to the definitions of the sensor model during data import. The experimental evaluations of ALOS PRISM imagery discussed, which cover test field applications in Australia and Bhutan, demonstrate that the model is capable of sub-pixel level geopositioning accuracy.

Keywords: sensor orientation model, ALOS PRISM, geopositioning, BARISTA

1. INTRODUCTION

There have been a number of sensor orientation models developed for pushbroom satellite imaging sensors, these having ranged from empirical models, through camera replacement models such as the now popular rational function model, to rigorous parametric formulations that model the physical image-to-object space transformation. In the case of vendor supplied rational polynomial coefficients (RPCs), it has now been well established that no loss in accuracy is to be expected when bias-corrected RPCs are used for georeferencing (eg [1]). However, not all vendors provide RPCs, and alternative empirical models are not always applicable. In such circumstances, a sensor model that takes full account of the physical reality of the imaging process needs to be employed, especially when the highest accuracy is sought.

In the case of pushbroom scanners, account must be taken of the fact that each image line has its own exterior orientation, albeit one that is highly correlated with adjacent scan lines. A popular sensor orientation modelling approach for satellite line scanners is to use time-dependant models for the platform position and attitude angles, but there are also other orbit models such as circular curves [2] or ellipses [3]. Given the increasing number of high-resolution imaging satellites being deployed, the attraction of applicable generic sensor orientation models is becoming more compelling. One such model [4] uses second-order piecewise polynomial functions to model the sensor trajectory and attitudes. Generic models, while being general, typically require satellite orbit and attitude data, which when available is provided by the satellite vendors in metadata files. Unfortunately, although the sensor geometry is basically the same for all pushbroom scanners, the formats and definitions of these metadata are not always compatible.

This paper presents the results of experimental applications of a new, generic sensor orientation model for pushbroom imaging sensors to ALOS PRISM imagery. The model, which is fully described in [5] and [6] is the result of a comprehensive analysis of the metadata information provided by various vendors and it is applicable to a number of current high-resolution satellite imaging systems. Within the new model, vendor-specific definitions related to sensor orientation are mapped to the general model at the time the metadata is imported, and the metadata is used to initialise the model parameters. The orbit and attitudes are then modelled by cubic splines. Although direct georeferencing is supported via the metadata and orbit and attitude modelling, compensation of systematic errors inherent in this data is needed for precise georeferencing. This is achieved through a least squares bundle adjustment incorporating additional parameters for the error modelling. A small number of ground control points (GPCs) is then needed to recover the error-corrected sensor orientation.

* Modified version of the paper *Application of a Generic Sensor Orientation Model to SPOT 5, Quickbird and ALOS Imagery* presented at the 28th Asian Conference on Remote Sensing, Kuala Lumpur, November 2007.

In the following sections, a review of the new sensor model will first be presented. The mapping of vendor-specific definitions to the generic model for ALOS PRISM is then described, after which results of experimental application of the model to precise georeferencing of ALOS imagery for test sites in Melbourne, Australia and Bhutan will be presented. The BARISTA software system for metric information extraction from satellite imagery [7] has been employed for the experimental evaluation.

2. REVIEW OF NEW GENERIC MODEL

2.1 Coordinate Systems and Transformations

The overview commences with consideration of the coordinate systems involved in the image-to-object space transformation. First, there is the *object coordinate system*, a 3D earth-centred Cartesian system [$\mathbf{X}_{ECS}$], which can be in earth centered reference system, eg WGS84. Next, there is the *orbital coordinate system* [$\mathbf{X}_O$], which is a time-dependant system with its origin defined by the satellite position $\mathbf{S}(t)$ at time t. The axes are defined so that the Z_O-axis is parallel to $\mathbf{S}(t_c)$, where t_c is the acquisition time at the scene centre. The Y_O-axis is orthogonal to both $\mathbf{S}(t_c)$ and the velocity vector at time t_c, $\mathbf{V}(t_c)$. The *platform coordinate system* [$\mathbf{X}_P$] is fixed to the satellite. The transformation between platform and orbit systems is a time-dependant rotation that can be parameterized by the three angles of *roll*, *pitch* and *yaw*.

Turning now to the satellite body, there is the *camera coordinate system* [$\mathbf{X}_C$]. This has its origin at the projection centre, with the the X_C-axis being parallel to the CCD array. The relationship between the camera and the platform system is given by the time-constant camera mounting parameters. There is also the *framelet coordinate system* [$\mathbf{X}_F$] in which the actual image coordinates (x_F,y_F) are measured. This system is shifted but not rotated relative to the camera system so that its origin is at the centre of the leftmost pixel of the CCD array. Finally, there is the *image file coordinate system* [$\mathbf{X}_I$] defined by the rows and columns of the image. Figure 1 shows the coordinate relationships for the camera body and the platform system.

The sensor model needs to describe the transformation of a point $\mathbf{P}_{ECS} = (X_{ECS}, Y_{ECS}, Z_{ECS})^T$ in the object coordinate system into the position of its projection $\mathbf{p}_I = (x_I, y_I, 0)^T$ in the image file coordinate system. Measuring an image point $\mathbf{p}_I$ immediately delivers the corresponding point $\mathbf{p}_F$ in the framelet coordinate system:

$$\mathbf{p}_F = (x_F, y_F, z_F)^T = (x_I, 0, 0)^T \quad (1)$$

The coordinate y_I establishes the time t at which the line containing the point was recorded, the time parameters of first-line acquisition time and line interval being obtained from the metadata. Taking into account the interior orientation, $\mathbf{c}_F = (x_F^C, y_F^C, f)^T$, the camera coordinates of the image point become $\mathbf{p}_C = \mathbf{p}_F - \mathbf{c}_F$. Thus, the relationship between the object point $\mathbf{P}_C$ in the camera coordinate system and the image point $\mathbf{p}_F$ in the framelet coordinate system becomes

$$\mathbf{P}_C = (X_C, Y_C, Z_C)^T = \lambda \cdot (\mathbf{p}_F - \mathbf{c}_F + \delta\mathbf{x}) \quad (2)$$

where λ is a scale factor describing the position of $\mathbf{P}_C$ along the image ray and $\delta\mathbf{x}$ is a vector of systematic error corrections. In the current formulation, $\delta\mathbf{x}$ comprises correction terms for velocity aberration and atmospheric refraction. In order to transform $\mathbf{P}_C$ to the platform system, the camera mounting parameters are then applied in the form of a rigid motion.

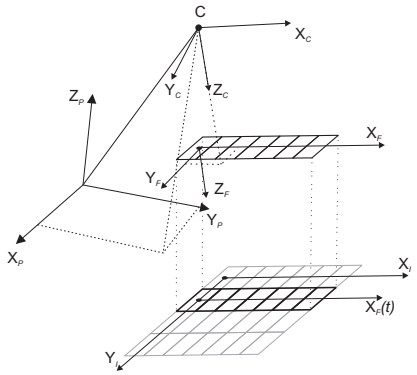

Figure 1. Coordinate systems [$\mathbf{X}_P$], [$\mathbf{X}_C$], [$\mathbf{X}_F$] and [$\mathbf{X}_I$].

The mounting parameters are the position $\mathbf{C}_M$ of the projection centre in the platform system, and the matrix $\mathbf{R}_M$ describing the rotation from the camera to the platform system. The platform and orbital systems are then related by a time-dependant rotation:

$$\mathbf{P}_O = (X_O, Y_O, Z_O)^T = \mathbf{R}_P(t)\,(\mathbf{C}_M + \mathbf{R}_M \cdot \mathbf{P}_C) \quad (3)$$

The rotation matrix $\mathbf{R}_P(t)$ is parameterised by the three rotations of *roll*, *pitch* and *yaw*, which change with time. Finally, the relationship between the object coordinates $\mathbf{P}_{ECS}$ and the orbit coordinates $\mathbf{P}_O$ is described by a rigid motion with a time-constant rotation matrix $\mathbf{R}_O$ and a time-dependant shift given by the satellite position $\mathbf{S}(t)$:

$$\mathbf{P}_{ECS} = (X_{ECS}, Y_{ECS}, Z_{ECS})^T = \mathbf{S}(t) + \mathbf{R}_O \cdot \mathbf{P}_O \quad (4)$$

A combination of Eqs. 2 to 4 yields the required transformation equation relating the image point $\mathbf{p}_F$ in the framelet coordinate to the object point $\mathbf{P}_{ECS}$ in the object coordinate system:

$$\mathbf{P}_{ECS} = \mathbf{S}(t) + \mathbf{R}_O \cdot \mathbf{R}_P(t) \cdot [\mathbf{C}_M + \lambda \cdot \mathbf{R}_M\,(\mathbf{p}_F - \mathbf{c}_F + \delta\mathbf{x})] \quad (5)$$

2.2 Modelling of Orbit and Attitude

The components $X(t),Y(t),Z(t)$ of the satellite orbit $\mathbf{S}(t)$ and the angles $roll(t)$, $pitch(t)$, $yaw(t)$ forming $\mathbf{R}_P$ are modelled by cubic splines $Sp^i_N(\bar{t}_i)$, with smooth transitions between segments i and $i+1$:

$$Sp^i_N(\bar{t}_i) = a^i_{N,0} + a^i_{N,1} \cdot \bar{t}_i + a^i_{N,2} \cdot \bar{t}_i^2 + a^i_{N,3} \cdot \bar{t}_i^3 \qquad (6)$$

Here, i is the index of the spline segment, N is the parameter modelled by the spline and $(a_{N,0}^i, a_{N,1}^i, a_{N,2}^i\ a_{N,3}^i)$ are the polynomial coefficients to be determined from orbit points and/or attitudes. Each polynomial $Sp^i_N(\bar{t}_i)$ models the parameter N for a time interval $[t_i^0, t_i^E]$ with $t_i^E = t_{i+1}^0$ being the time of transition between segments. At the interval limits, the two polynomials and their 1st and 2nd derivatives have to be identical, which results in three constraint equations per inner node $\bar{t}_{i+1}^0 = 0$ with $i \neq 0$ (see Weser et al., 2007; 2008).

Discrete orbit points and attitude observations are generally time stamped. For an orbit point $(X^{obs}, Y^{obs}, Z^{obs})^T$ recorded at time t^{obs}, the segment i of the orbit splines that this point belongs to can be determined and the relationship between the observed orbit coordinates and the orbit splines becomes:

$$\begin{aligned} F_X(X^{obs}, Y^{obs}, Z^{obs}, t^{obs}) &= X^{obs} + \Delta X = Sp^i_X(\bar{t}_i^{obs}) \\ F_Y(X^{obs}, Y^{obs}, Z^{obs}, t^{ob}) &= Y^{obs} + \Delta Y = Sp^i_X(\bar{t}_i^{obs}) \\ F_Z(X^{obs}, Y^{obs}, Z^{obs}, t^{ob}) &= Z^{obs} + \Delta Z = Sp^i_Z(\bar{t}_i^{obs}) \end{aligned} \qquad (7)$$

where F_X, F_Y and F_Z are functions modelling systematic errors in the orbit coordinates. The vector $(\Delta X, \Delta Y, \Delta Z)^T$ currently describes a systematic shift relative to the object coordinate system. The more general notation of F_X, F_Y, and F_Z indicates that this model is expandable, for instance by rotations or time-dependant terms. An analogous model is used for the attitudes. Perturbations in the observed rotation angles $(roll^{obs}, pitch^{obs}, yaw^{obs})^T$ are modelled by time-constant offsets $(\Delta roll, \Delta pitch, \Delta yaw)^T$, a model that could also be expanded.

2.3 Systematic Error Compensation

Within the functional model formed by the combination of Eqs. 5 and 6, which is solved via least-squares adjustment, the observations comprise the framelet coordinates $\mathbf{p}_F$. The parameters include the corrections to the image coordinates $\delta\mathbf{x}$ (not always carried as unknowns); the polynomial coefficients $a_{N,0}^i$, $a_{N,1}^i$, $a_{N,2}^i$ and $a_{N,3}^i$ of the splines modelling the three components of the orbit $\mathbf{S}(t)$ and the three angles by which $\mathbf{R}_P(t)$ is parameterised; and the positions $\mathbf{P}_{ECS}$ of the GCPs. The GCP coordinates can also be treated as direct observations. In addition, there are unknown parameters associated with the spline segment constraint equations. For the direct observations of the orbit points, the combination of Eqs. 6 and 7 provides the functional model. The observations in these equations are the orbit point coordinates (X^{obs}, Y^{obs}, Z^{obs}) and the observed rotations ($roll^{obs}$, $pitch^{obs}$, yaw^{obs}). The polynomial coefficients of the orbit and attitude splines also constitute unknown parameters. With respect to the bias correction parameters (ΔX, ΔY, ΔZ and $\Delta roll$, $\Delta pitch$, Δyaw), they can be considered as either constants or unknowns.

3. MAPPING OF DEFINITIONS FOR ALOS

The transformation process between object and image space for ALOS PRISM imagery can be expressed by an equation that is very similar to Eq. 5, except that there is only one rotation relating the platform and object coordinate systems, and this rotation matrix is parameterised by quarternions. The equation follows as

$$\mathbf{P}_{ECS} = \mathbf{S}(t) + \mathbf{R}_A(t) \cdot [\mathbf{C}_M + \lambda \cdot \mathbf{R}_M \cdot (\mathbf{p}_F - \mathbf{c}_F + \delta\mathbf{x})] \qquad (8)$$

Where computation of the rotation matrix $\mathbf{R}_O$ utilises the identity $\mathbf{R}_O \cdot \mathbf{R}_P(t) = \mathbf{R}_A(t)$, resulting in

$$\mathbf{R}_P(t) = \mathbf{R}_O^T \cdot \mathbf{R}_A(t) \qquad (9)$$

ALOS PRISM displays a significant characteristic regarding the framelet coordinate system. Depending on the viewing mode, either four or six CCD arrays are used to record the digital image. For basic imagery, one image data file per CCD array is provided. We refer to this here as a sub-image. Figure 2 shows the layout of four such CCD arrays, there being an individual framelet coordinate system for each. All parameters in the model of Eq. 5 are identical for each of these framelet coordinates except the coordinates of the principal point (x_F^C, y_F^C). These differ by a constant offset, defined by the width of the CCD arrays and the nominal overlap of 32 pixels.

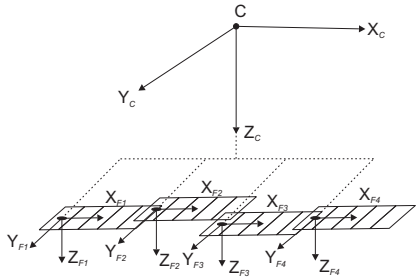

Figure 2. CCD array configuration of ALOS Prism.

4. EXPERIMENTAL EVALUATION

4.1 Test data

Two test field data sets were employed in the experimental evaluation of the generic sensor model

applied to ALOS PRISM 2.5m resolution imagery. The first covered an already established test field in Melbourne, Australia [1]. The test area of 40 x 49 km^2 has relatively flat terrain with heights between sea level and 200 m and it comprises some 130 GPS surveyed GCP/check points to 20 cm accuracy in planimetry and 40 cm in height. The majority of GCPs are road roundabouts or road intersections, which have proved suitable for the 2.5 m resolution ALOS imagery.

The second ALOS imagery data set covered an area of 60 x 60 km^2 in Bhutan, the test field comprising 29 GCPs which could be used as either control points in the bundle adjustment or check points. The distribution of the points was not optimal due to both restricted accessibility of the terrain and the fact that the GCPs were initially established to support experimental application of the sensor model to SPOT 5 imagery. Points were mainly located along roads on valley floors, with a few on passes, the overall height range for the ALOS GCPs being from 600 m. The accuracy of the GPS coordinates was again around ±0.2 m in planimetry and ±0.4 m in height.

Four panchromatic sub-images (1 per CCD array) for each of the Forward, Nadir and Backward views were employed in the Melbourne test field, resulting in a 12-image network. The same configuration was planned for the Bhutan data set, but four sub-images could not be employed due to the extent of cloud cover in each. Thus, the Bhutan network comprised eight sub-images, three backward, three nadir and two forward.

4.2 Results

All computations for the new generic sensor orientation model were performed within the BARISTA software system, which can accommodate georeferencing from multi-image and multi-sensor network configurations [7]. In order to assess the effectiveness of the sensor orientation adjustment model, image coordinates of check points were measured in all sub-images. In the Melbourne data set, the results for the sub-images of each scene were averaged. Check points were then back-projected into the images using the original parameters of the sensor model, i.e. those derived by mapping the vendor-specific parameters to the model. RMS values of the resulting image coordinate differences were then computed as a quality measure in image space of the direct georeferencing.

For the sensor orientation adjustment, three orbit/attitude correction model combinations were employed: an orbit shift only correction, an attitude only corrections and a combination of both. Once again, resulting check point coordinates were back-projected into the images, this time using the estimated sensor orientation parameters. The RMS values of the image coordinate differences were then computed. All resulting RMS values are listed in Table 1, from which the significant improvement of the generic sensor model over the direct georeferencing solution can be clearly seen.

Table 1. RMS discrepancies between back-projected and measured image coordinates, in pixels, Melbourne data.

RMS errors in image coordinates		ALOS (7 GCPs, 122 Chkpts)		
		Nadir	Backward	Forward
Direct geo-referencing	x	29.31	24.95	29.67
	y	1.62	8.59	5.81
Orbit Path Correction	x	0.91	0.90	0.90
	y	0.67	0.80	0.96
Orbit Attitude Correction	x	1.03	0.91	0.87
	y	0.64	0.82	0.80
Orbit Path + Attitude Corrn.	x	0.91	0.90	0.89
	y	0.69	0.83	0.79

The RMS coordinate errors shown in Table 1 for direct georeferencing are in the range of 2 to 30 pixels, thus highlighting the importance of correcting the systematic errors in order to exploit the full metric potential of the ALOS imagery. Bias correction improves the results considerably; the RMS discrepancy values reduce to a range of 0.6 to 1.0 pixels. This illustrates that subpixel accuracy can be achieved for well-defined ground feature points. Interestingly, the results are basically equivalent for each of the bias-compensation cases, which is likely attributable to the fact that the orbit and attitude correction parameters cannot be projectively well separated when a small number of GCPs is used. The RMS error values in Table 1 are slightly higher than anticipated, which is attributable to the often poorer than desirable definition of ground feature points in the ALOS images. The result is higher random measurement error, with there being no indication of significant remaining bias in the parameters of the sensor model.

In order to assess the absolute accuracy of georeferencing via the new model, RMS error values were computed at all check points, the object coordinates from the adjustment process being compared to the observed GPS coordinates within the UTM reference system. Tables 2 and 3 list the results

for the Melbourne and Bhutan networks, with the listed discrepancies being for planimetry and height. Results are shown for the case of Orbit Path Correction (shift only), for varying numbers of GCPs.

Table 2. Geopositioning accuracy for Melbourne ALOS 12 sub-image data set using orbit path correction.

Number of GCPs / Checkpts	RMSE in planimetry, S_{XY} (m / pixels)	RMSE in height, S_Z (m / pixels)
4 / 125	2.2 / 0.9	2.5 / 1.0
7 / 122	1.8 / 0.7	2.4 / 1.0
10 / 119	1.9 / 0.8	2.3 / 0.9
20 / 109	1.8 / 0.7	2.3 / 0.9

Table 3. Geopositioning accuracy achieved for Bhutan ALOS 8 sub-image data set using orbit path correction.

Number of GCPs / Checkpts	RMSE in planimetry, S_{XY} (m / pixels)	RMSE in height, S_Z (m / pixels)
4 / 25	2.3 / 0.9	3.4 / 1.4
7 / 22	2.3 / 0.9	3.0 / 1.2
10 / 19	2.2 / 0.9	3.0 / 1.2
12 / 17	2.3 / 0.9	2.9 / 1.2

Overall, the georeferencing accuracy achieved for the 2.5 m ALOS PRISM imagery is close to 1 pixel in both test fields, with the results for Melbourne being better than those for Bhutan as a consequence of the better GCP/checkpoint definition and image measurement accuracy in the Melbourne imagery. Further details regarding the results from the Melbourne test field are provided in [6].

5. CONCLUSIONS

The results of testing a new generic pushbroom sensor model applicable to ALOS PRISM imagery have been presented. The new sensor orientation model is also applicable to most other pushbroom scanners, so long as the vendor-specific parameterisation of the object-to-image coordinate transformations can be mapped to those of the model. The new model, which allows orbit and attitude correction, has yielded a 1-pixel or better bias-free georeferencing accuracy for ALOS PRISM in cases where as few as half a dozen or so GCPs are employed.

6. REFERENCES

[1] Fraser, C.S. & Hanley H.B., 2003. Bias Compensation in Rational Functions for IKONOS Satellite Imagery. *Photogrammetric Engineering & Remote Sensing*, 69(1): 53-57.

[2] Dowman, I., Michalis P., 2003. Generic rigorous model for along track stereo satellite sensors. *Proceedings of ISPRS Workshop "High Resolution Mapping from Space 2003"*, Hannover, Germany. Proceedings on CDROM.

[3] Westin, T. 1990. Precision Rectification of SPOT Imagery. *Photogrammetric Engineering & Remote Sensing*, 56(2): 247-253.

[4] Poli, D., 2005. Modelling of Spaceborne Liner Array Sensors. *Ph. D. Dissertation, IGP Report No. 85*, Institute of Geodesy and Photogrammetry, ETH Zurich, Switzerland.

[5] Weser, T., Rottensteiner, F., Willneff, J. and Fraser, C.S., 2007. A Generic Pushbroom Sensor Model for High-Resolution Satellite Imagery Applied to Spot 5, QuickBird and ALOS Data Sets. *Intern. Arch. of Photogramm., Remote Sens. & Spatial Inform. Sc. (Eds. C. Heipke, K. Jacobsen & M. Gerke)*, Hannover, Germany, Vol. 36, Part I/W51, 6 pages (on CD-ROM)

[6] Weser, T., Rottensteiner, F., Willneff, J., Poon, J. and Fraser, C.S., 2008. Development and Testing of a Generic Sensor Model for High-Resolution Satellite Imagery. *Photogrammetric Record*, 21 pages (in press).

[7] Willneff, J., Poon, J. & Fraser, C.S., 2005. Single-Image High-Resolution Satellite Data for 3D Information Extraction. *Intern. Arch. of Photogramm., Remote Sens. & Spatial Inform. Sc. (Eds. C. Heipke, K. Jacobsen & M. Gerke)*, Hannover, Germany, Vol. 36, Part I/W3, 6 p. (CD-ROM).